

## Sensitivity Study of IceCube-Gen2 Surface Array for Cosmic-Ray Anisotropy

---

**Wenjie Hou for the IceCube-Gen2 Collaboration<sup>a,\*</sup>**

<sup>a</sup>*Institute for Astroparticle Physics, Karlsruhe Institute of Technology (KIT),  
D-76021 Karlsruhe, Germany*

*E-mail:* [wenjie.hou@kit.edu](mailto:wenjie.hou@kit.edu)

One of the major unresolved issues in cosmic-ray physics is the transition from galactic to extragalactic origin. Pinpointing the exact energy of this transition remains a challenge, as the trajectories of CRs are significantly influenced by the magnetic fields present in the Galaxy, making it difficult to trace individual CRs back to their specific origins. However, constraints can be obtained by studying the cosmic-ray anisotropy in the energy range from PeV to EeV where the transition is expected to occur. The sensitivity to cosmic-ray anisotropy is in particular a matter of statistics. With the upcoming IceCube-Gen2 surface array, which will cover 8 times more area than the existing IceTop surface array, there will be an increase in statistics and capability to investigate cosmic-ray anisotropy with higher sensitivity. We will present performed simulation studies of the sensitivity to the cosmic-ray anisotropy signal expected with the IceCube-Gen2 surface array.

*XVIII International Conference on Topics in Astroparticle and Underground Physics (TAUP2023)  
28.08-01.09.2023  
University of Vienna*

---

\*Speaker

## 1. Introduction

One of the most significant unresolved questions in cosmic-ray (CR) physics pertains to the energy at which the transition from Galactic to extragalactic cosmic rays occurs, as CRs are deflected by the Galactic magnetic fields, which result in their unclear origins. However, constraints can be obtained by studying the large-scale anisotropy in the CR arrival directions. In the past few decades, experiments have provided long-term and significant observations of a subtle sidereal anisotropy with the dipole magnitude ranging from  $10^{-4}$  to  $10^{-2}$ , and across a wide energy range from 1 TeV to 100 EeV [1–12]. However, statistically significant measurements of the projected dipole amplitude are missing in the energy range between 10 PeV and 1 EeV [2, 11, 13]. IceCube-Gen2 [14], and its surface array (comprised of stations of elevated scintillation and radio detectors) will be capable of filling a portion of the energy gap between 1 PeV and approximately 100 PeV. Here, we present the air-shower reconstruction efficiency for the scintillators of the planned IceCube-Gen2 surface array using CORSIKA simulations [15], describe the Monte Carlo studies of the CR arrival directions, and show the sensitivity of the surface array to large-scale anisotropy of the CRs [16].

## 2. Reconstruction efficiency of the IceCube-Gen2 surface array

The planned surface area covered by the IceCube-Gen2 surface array is 6.6 km<sup>2</sup>. The corresponding CORSIKA simulations of the scintillator array response were performed for proton- and iron-induced air showers with  $4 \leq \log_{10}(E/\text{GeV}) \leq 8$  and zenith angles ( $\theta$ ) up to  $51^\circ$ , and  $4 \leq \log_{10}(E/\text{GeV}) \leq 7.5$  with  $\theta$  up to  $63^\circ$  [15] (see Figure 1).

To show the detector's realistic capabilities, we perform a selection process that involves choosing true air shower core locations within 100 meters of the surface array's polygonal edge, giving an area of 5.22 km<sup>2</sup> large, which can be treated as a containment cut. For a simple air

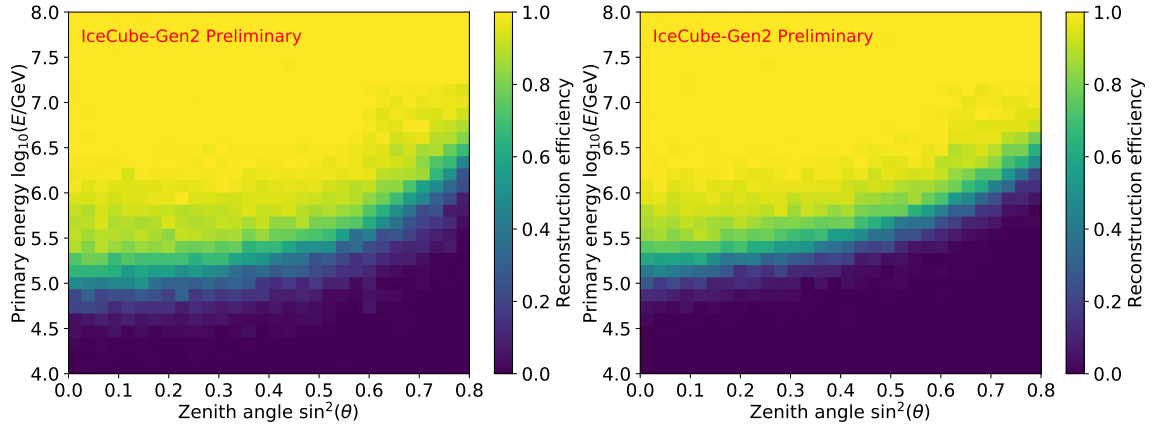


**Figure 1:** 2D histograms of the reconstruction efficiency for proton- (left) and iron- (right) induced air shower for scintillators in the IceCube-Gen2 surface array, with energy range from  $10^6$  GeV to  $10^8$  GeV, zenith angle up to  $63^\circ$  in  $\sin^2 \theta$  scale, and scintillator multiplicity  $\geq 5$  to trigger the event.

shower trigger, at least 3 hits within the array are required in order to roughly reconstruct the shower geometry. A more realistic requirement in the context of air shower reconstruction is 5 triggered scintillator detectors. Considering the scintillator triggered multiplicities  $\geq 5$ , we get the

reconstruction efficiencies for proton and iron primaries and fit the results with a modified error function of the energy  $E$  and the zenith angle with  $z = \sin^2 \theta$ :

$$\epsilon(E, z) = \frac{1}{2} \left[ 1 + \operatorname{erf} \left( \frac{E - (\mu_0 + \mu_1 z + \mu_2 z^2 + \mu_3 z^3)}{\sigma_0 + \sigma_1 z} \right) \right], \quad (1)$$

and the polynomials in the error function (erf) up to the third order ( $z^3$ ) can capture sufficient details for reconstruction efficiencies. The corresponding contour lines represent 50% and 98% of the reconstruction efficiencies for proton, iron, and the total efficiency are shown in Figure 2. Based on the logarithmic mass dependence of the cosmic-ray primaries, we estimate the reconstruction efficiencies for helium, nitrogen, and aluminum:

$$\epsilon(A_i, E, z) = \frac{\ln A_i}{\ln A_{\text{Fe}} - \ln A_{\text{P}}} [\epsilon_{\text{Fe}}(E, z) - \epsilon_{\text{P}}(E, z)] + \epsilon_{\text{P}}(E, z), \quad (2)$$

where  $i$  ranges from 1 to 3, representing the estimated helium, nitrogen, and aluminum respectively.

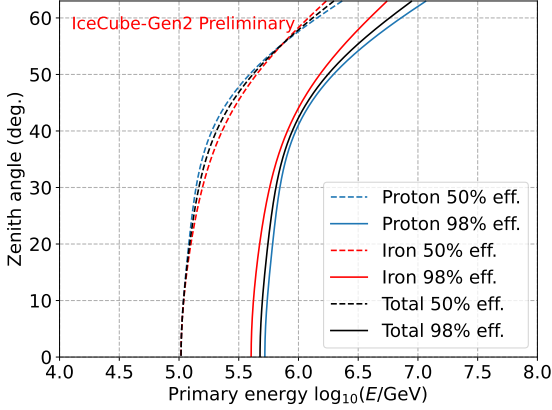


**Figure 2:** Contour lines with 50% and 98% reconstruction efficiency of the IceCube-Gen2 surface array are shown for proton and iron. The total efficiency of all particles utilizes the H4a flux model [17].

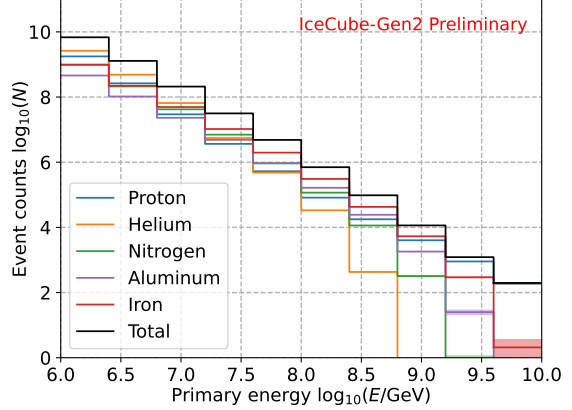


**Figure 3:** Histogram of the event counts of the IceCube-Gen2 surface array with a 10-year exposure, considering the H4a flux model and the reconstruction efficiency with 3 additional energy bins.

### 3. Monte-Carlo simulation of cosmic-ray arrival directions

We now apply the detection efficiency to simulate the arrival directions for the IceCube-Gen2 surface array with a 10-year exposure. Worth noticing that the exposure time of Gen2 is equivalent to the exposure time in the current IceTop years. However, the IceCube-Gen2 surface array has an increased surface area, being 8 times larger than IceTop, but the statistics of the IceCube-Gen2 surface array are not simply 8 times that of IceTop's, and its reconstruction efficiencies of cosmic-ray primaries differ. The simulation is divided into 7 energy bins which range from  $10^6$  GeV to  $10^{8.8}$  GeV with a bin size of 0.4 in  $\log_{10}(E/\text{GeV})$ . Using the H4a flux model [18], the number of arrival directions in each energy bin can be calculated by integrating the efficiency (with  $\theta$  from  $0^\circ$  to  $63^\circ$ ) obtained respectively by Eq.(1) and the number of cosmic rays with 10 years of exposure of

the surface array. Therefore, we have the effective event counts of cosmic-ray primaries for each of the 5 primary components in all the energy bins (also see the histogram shown in Figure 3):

$$N_{\text{eff},ij} = \int_{\theta_{\min}}^{\theta_{\max}} \int_{E_{j-1}}^{E_j} \epsilon_i(E, \theta) N_{\text{H4a},i}(E) dE d\theta, \quad (3)$$

where  $i$  ranges from 1 to 5 represent the 5 primary particles,  $j$  ranges from 1 to 8 for the edges of the 7 energy bins, and  $N_{\text{H4a},i}$  represents the event count for each of the 5 primary particles using the H4a flux mode. In total, we have 8.36 billion simulated cosmic-ray events over all 7 energy bins. Taking into account the ratio of different primaries weighted by the mass-dependent H4a flux [18] and Eq.(1), the total efficiency averaged over all primaries is written as

$$\epsilon_{\text{tot}}(E, \theta) = \frac{\sum_{i=1}^5 \epsilon_i(E, \theta) \phi_{\text{H4a},i}(E)}{\sum_{i=1}^5 \phi_{\text{H4a},i}(E)}. \quad (4)$$

Next, we randomly inject 15 dipoles with different amplitudes in each energy bin and scan over the dipole declination from  $-80^\circ$  to  $80^\circ$  with a bin size of  $10^\circ$ . It is irrelevant whether the dipole orientation is within or outside the field of view (FoV) of Gen2. Furthermore, any observatory situated on Earth will invariably detect a partial sky coverage CR dipole, with the dipole orientation, or 'hotspot', potentially located either within or outside the FoV. In the simulation, we have a total of 1785 injected dipole maps, each with amplitudes detectable at levels exceeding  $10\sigma$ . Our goal is to study how dipole significance propagates at IceCube-Gen2, so we consistently use larger amplitudes as inputs. Therefore, the amplitudes are chosen from 0.007 up to 0.956 for the dipoles with different energy bins covering different ranges of amplitude. The distribution function of CRs is a function of the exposure of IceCube-Gen2 surface array with a dipole and the reconstruction efficiency,

$$\omega_{\text{Gen2}}(E, \theta, \theta_{\max}, \mathcal{A}, \delta_d, \delta_{\text{Gen2}}) = \omega(\theta, \theta_{\max}, \delta_{\text{Gen2}}) \times \epsilon_{\text{tot}}(E, \theta) \times \mathcal{D}(\mathcal{A}, \delta_d, \delta_{\text{Gen2}}), \quad (5)$$

where  $\delta_d$  denotes the dipole declination,  $\omega$  is the relative exposure of an observatory at declination  $\delta_{\text{Gen2}} = -89.99^\circ$ , the function  $\mathcal{D}(\mathcal{A}, \delta_d, \delta_{\text{Gen2}})$  provides the dipole distributions.

#### 4. Sensitivity to the cosmic ray anisotropy

To assess the sensitivity of a partial-sky coverage observatory to a dipole anisotropy, it is essential to compare the actual sky map  $N_{\text{pix},i}$  of injected CR arrival directions by Eq.(5) with a reference map  $\langle N \rangle_{\text{pix},i}$  without dipole, and generate sky maps of relative intensity within the FoV with  $I = (N_{\text{pix},i} - \langle N \rangle_{\text{pix},i}) / \langle N \rangle_{\text{pix},i}$ . Then, we perform a one-dimensional (1D) projection of the sky map and fit it with a first harmonic function  $\mathcal{A}_{\text{reco}} \cos(n(\alpha - \phi)) + B$ , where  $\mathcal{A}_{\text{reco}}$  is the amplitude of the reconstructed dipole,  $\phi$  is the phase, and  $B$  is a constant. The reconstruction ratio between the reconstructed dipole and the true input dipole ( $\mathcal{A}_{\text{reco}}/\mathcal{A}$ ) in the majority of the cases are below 80% due to the limited FoV of the surface array.

To assess the significance of a dipole deviation from isotropy, we consider the deviation from a null hypothesis in the number of sigmas  $n_\sigma = (\mathcal{A}_{\text{reco}} - \mathcal{A}_{\text{hypo}}) / \sigma_{\mathcal{A}}$ , where  $\mathcal{A}_{\text{hypo}}$  is set to 0, representing the expected value under the null hypothesis. We assume that the  $\sigma_{\mathcal{A}}$  of the dipole amplitude reconstruction is proportional to  $1/\sqrt{N}$  and verified this through Monte Carlo simulation

and the covariance matrix in the first harmonic fit of the 1D projected map. Therefore, the sensitivity function (propagation of sigmas) can be expressed as:

$$n_\sigma = \mathcal{S}(\mathcal{A}, E, \theta_{\max}, \delta_d, \delta_{\text{Gen2}}) \mathcal{A} \sqrt{N}, \quad (6)$$

where  $\mathcal{S}$  is defined as a sensitivity coefficient. We need to clarify that the sensitivity to the true dipole, denoted as  $n_\sigma = \mathcal{S}_{\text{true}} \mathcal{A}_{\text{true}} \sqrt{N}$ , is the corresponding true dipole of  $3\sigma$  or  $5\sigma$  reconstructed dipole  $n_\sigma = \mathcal{S}_{\text{reco}} \mathcal{A}_{\text{reco}} \sqrt{N}$ . We scatter the data points ( $n_\sigma/\sqrt{N}, \mathcal{A}$ ) for both the reconstructed dipole and true dipole cases from the simulation and fit the points with a polynomial equation of the form  $\sum_{i=1}^3 \lambda_i \mathcal{A}^i$ , where  $\lambda_i$  are the coefficients of the polynomials. The slopes of these curves represent the sensitivity coefficients for both the reconstructed and true dipole cases:

$$\mathcal{S}(\mathcal{A}, E) = \lambda_1(E) + 2\lambda_2(E)\mathcal{A} + 3\lambda_3(E)\mathcal{A}^2, \quad (7)$$

where  $\lambda_1, \lambda_2$  and  $\lambda_3$  are parameters for proton and iron which are energy dependent.

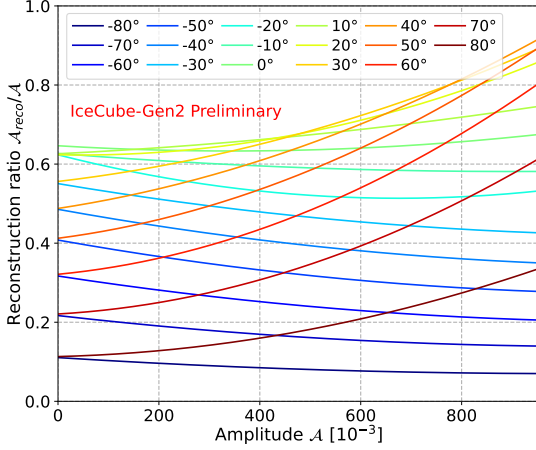


**Figure 4:** Ratio between reconstructed dipole and true dipole in the Monte-Carlo simulation. The true amplitude ranges from 0.007 to 0.956, while the declination ranges from -80 degrees to 80 degrees. However, different energy bins cover different ranges of the true dipole amplitude.

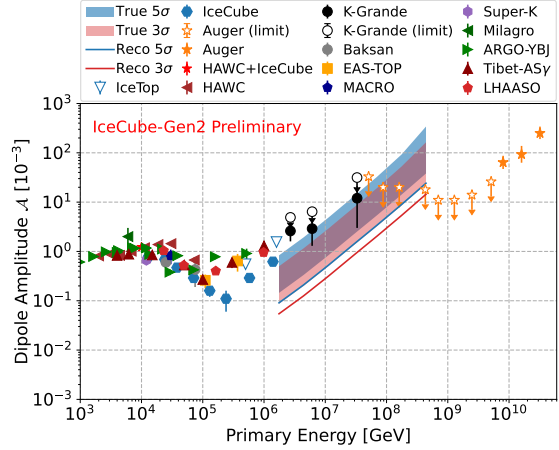


**Figure 5:** The curves show the  $3\sigma$  and  $5\sigma$  sensitivity of the IceCube-Gen2 surface array to the reconstructed dipole, bands show the corresponding true dipole of the  $3\sigma$  and  $5\sigma$  reconstructed dipole. The data points shown are reconstructed dipole amplitudes from the various experiments [1–12].

Taking into account the energy gap region with upper limits and the highest energy data from IceCube, the energy range chosen for this work is from  $10^6$  GeV to the overlap region with Auger, approximately around  $10^{8.8}$  GeV. Figure 4 shows the ratio between the reconstructed dipole and the true dipole. The  $3\sigma$  and  $5\sigma$  sensitivity curves of the reconstructed dipole and bands of the corresponding true dipole of the IceCube-Gen2 surface array are shown in Figure 5, which represents the significance of a deviation from the null hypothesis.

## 5. Conclusion and outlook

We present the 2D function of the air shower reconstruction efficiency of proton and iron primaries for the IceCube-Gen2 surface array based on the existing CORSIKA simulation and

estimate the reconstruction efficiencies for helium, nitrogen, and aluminum. Next, we simulate the CR arrival directions for the surface array using Monte-Carlo simulation by injecting 1785 dipoles in 7 energy bins with different declinations. To assess the anisotropy, we compare a dipole map with a reference map for all cases, make the sky maps of relative intensity, and perform 1D projections of the sky maps and fit them with the first harmonics. To assess the sensitivity of the surface array to a dipole anisotropy, we consider a null hypothesis and the propagation of the sigmas. Finally, we show the  $3\sigma$  and  $5\sigma$  sensitivity to the CR dipole anisotropy with curves and bands (Fig.5). With IceCube-Gen2, it will be possible to improve the sensitivity of the CR anisotropy in the energy range of the galactic-extragalactic transition of the CR origin. The sensitivity studies will be extended in the future, in particular by more realistic simulations. For example, we can perform simulations with limited dipole orientations (by KASCADE-Grande and Auger) as inputs, conduct simulations with multipole moments, and investigate the sensitivity of IceCube-Gen2 surface array to both isotropic and multipole anisotropy.

## References

- [1] **HAWC** Collaboration, A. U. Abeysekara *et al.* *Astrophys.J.* **865** no. 1, (2018) 57.
- [2] **KASCADE-Grande** Collaboration, A. Chiavassa *et al.* *PoS ICRC2015* (2015) 281.
- [3] **EAS-TOP** Collaboration, M. Aglietta *et al.* *Astrophys.J.Lett.* **692** (2009) 130–133.
- [4] **MACRO** Collaboration, M. Ambrosio *et al.* *Phys.Rev.D* **67** (2003) 042002.
- [5] **Super-Kamiokande** Collaboration, G. Guillian *et al.* *Phys.Rev.D* **75** (2007) 062003.
- [6] **Milagro** Collaboration, A. A. Abdo *et al.* *Astrophys.J.* **798** (2009) 2121–2130.
- [7] **Argo-YBJ** Collaboration, B. Bartoli *et al.* *Astrophys.J.* **809** no. 1, (2015) 90.
- [8] **Tibet** Collaboration, M. Amenomori *et al.* *Astrophys.J.Lett.* **626** (2005) 29–32.
- [9] **IceCube** Collaboration, M. G. Aartsen *et al.* *Astrophys.J.* **765** (2013) 55.
- [10] **IceCube** Collaboration, M. G. Aartsen *et al.* *Astrophys.J.* **826** no. 2, (2016) 220.
- [11] **Pierre Auger** Collaboration, A. Aab *et al.* *Astrophys.J.* **891** (2020) 142.
- [12] **LHAASO** Collaboration, W. Gao *et al.* *PoS ICRC2021* (2021) 351.
- [13] **KASCADE-Grande** Collaboration, A. Chiavassa *et al.* *Astrophys.J.* **870** no. 2, (2019) 91.
- [14] **IceCube-Gen2** Collaboration, M. G. Aartsen *et al.* *J.Phys.G* **48** no. 6, (2021) 060501.
- [15] **IceCube-Gen2** Collaboration, R. Abbasi *et al.* *PoS ICRC2021* (2021) 411.
- [16] **IceCube-Gen2** Collaboration, W. Hou *et al.* *PoS ICRC2023* (2023) 354.
- [17] P. Sommers *Astropart. Phys.* **14** (2001) 271–286.
- [18] T. K. Gaisser *Astropart. Phys.* **35** (2012) 801–806.